Supplementary Information for

Decoupling mechano- and electrochemical gating: A direct visualization for piezo-ionic propelled proton tunneling in self-charging supercapacitor

Karthikeyan Krishnamoorthy[1], Sindhuja Manoharan[1], Vimal Kumar Mariappan[1], Parthiban Pazhamalai[1], and Sang-Jae Kim[1,2,3,*]

[1]Nanomaterials & System Lab, Major of Mechatronics Engineering, Faculty of Applied Energy System, Jeju National University, Jeju 63243, Republic of Korea.

[2]Nanomaterials & System Lab, Major of Mechanical System Engineering, College of Engineering, Jeju National University, Jeju 63243, Republic of Korea.

[3]Research Institute of Energy New Industry, Jeju National University, Jeju 63243, Republic of Korea.

*Corresponding author Email address: kimsangj@jejunu.ac.kr

S1. Preparation of graphene oxide sheets:

The graphitic oxide sheets are prepared via modified Hummers method using the reaction between graphite powders, conc. H_2SO_4 and $KMnO_4$ as starting materials as reported in our earlier works [1]. The graphitic oxide sheets are redispersed in water and subjected to ultrasound irradiation using a probe type sonication (SONIC VCX 750 model (20 kHz, 750 W)) with a direct immersion titanium horn for 2 h that will result in the exfoliation of graphitic oxide into graphene oxide sheets. Finally, the graphene oxide sheets are centrifuged and dried at 80 °C for 12 h.

S2. Preparation of graphene sheets:

The graphene sheets are prepared via thermal reduction of graphene oxide in a tube furnace at high temperature [2]. Briefly, 1 g of as GO sheets was well grounded and annealed at a temperature of 900 °C (with a heating rate of 10 °C) for 2 h in an Ar atmosphere. After completion of the reaction, the furnace was allowed to cool naturally until it reaches the room temperature. Finally, a black colored powder was formed because of thermal reduction of GO into graphene sheets.

S3. Instrumentation:

An X-ray diffractometer system (Empyrean) with Cu-Kα radiation (λ = 1.5418 Å) is used to obtain the X-ray diffraction pattern of the GO and graphene sheets. The oxygenated functional groups present in GO before and after thermal treatment was analyzed using Fourier transform infra-red spectral analysis (Nicolet 6700 Thermo Fisher Scientific FT-IR spectrometer). Here, the GO or graphene sheets were pre-mixed powders with KBr were compressed into a pellet for

measurement using bare KBr as a reference. The chemical and surface state of elements present in the GO and graphene sheets were examined using an X-ray photoelectron spectrometer (ESCA-2000, VG Microtech Ltd.). Raman spectra of the GO and graphene sheets were acquired from a LabRAM HR Evolution Raman spectrometer (Horiba Jobin Yvon, France) using an argon ion laser with an excitation wavelength of 514 nm. The Raman mapping of the graphene sheets was performed over an area of $-2 \times 2\ \mu m^2$ comprising 100 spectral arrays and are analyzed using LabSpec (Ver. 6.2) software. The surface morphology and elemental mapping analysis were examined using FESEM (JSM-6700F, JEOL Instruments) and HRTEM (JEM-2011, JEOL). The topography and phase image of the nafion membrane were probed using an atomic force microscope equipped with kelvin probe force microscope with an applied bias voltage of +500 mV (AFM-KPFM, Digital Instruments, Nanoscope V multimode 8, Korea Basic Science Institute (KBSI), Jeonju Centre, South Korea.). The energy-harvesting properties of the Nafion film with metallic aluminum foil as the top and bottom electrodes (sealed using a moisture-resistant pouch) were measured on Keithley Electrometer (Model no: 6514) via varying the acceleration of the linear motor (LinMot E1100).

S4. Fabrication of graphene PI-SCSPC

The graphene PI-SCSPC device was fabricated on coating the graphene sheets on the surface of Nafion film via hot pressing method in a multi-step procedure. Briefly, graphene sheets and PVDF binder were mixed in the ratio 95:5 with and coated on the surface of insulating textile fabrics and allowed to dry at 80 °C for 12 h. Later, identical graphene coated textile fabrics are sandwiched using Nafion film and allowed to hot press at a temperature of 120 °C that results in the transfer of graphene electrodes on either side of the Nafion film.

S5. Electrochemical studies

Electrochemical studies, such as cyclic voltammograms, galvanostatic CD analysis, and electrochemical impedance spectroscopy of the fabricated SSCs, were performed on an AUTOLAB PGSTAT302N electrochemical workstation. The device capacitance, energy (E) and power (P) density of the graphene PI-SCSPC device were determined using the following relations [3]:

$$C_A = \int IdV / (s \times \Delta V \times A) \quad \text{..... (1)}$$

$$C_A = (I \times \Delta t) / (\Delta V \times A) \quad \text{..... (2)}$$

$$E = 0.5 \times Csp \times \Delta V^2 \quad \text{.....} \quad (3)$$

$$P = E / \Delta t \quad \text{.....} \quad (4)$$

Here "C_{sp}" is the device capacitance (F cm^{-2}), "I" is the current (A), "s" is the scan rate (mV s^{-1}), "ΔV" is the voltage window (V), "Δt" is the discharge time (s) and "A" is the area of the electrodes (cm^2).

S6. Measurement of electrochemical gating with mechanical stimulation:

The electrochemical gating effect was studied on the graphene PI-SCSPC using three-electrode configuration in which the two ends of the graphene SC electrode are used as source and drain terminals whereas the other graphene SC electrode is used as the gate terminal. The mechanical stimulation was given by a bending tester machine (JUNIL-JIBT-200). All the measurements related to electrochemical gating field effect transistor characterizations were performed on Agilent Semiconductor Parameter Analyzer (B1500A).

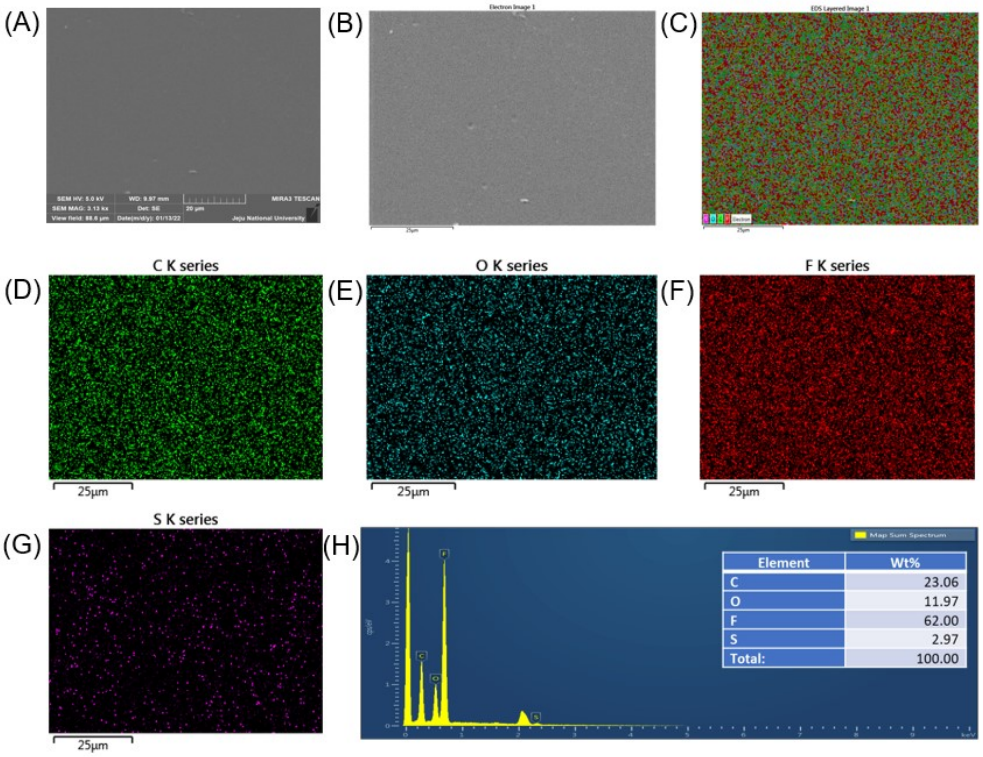

Figure S1. Morphological and elemental analysis of Nafion polyelectrolyte film. (A,B) FE-SEM micrograph of Nafion film recorded at a scale of 20, 25 µm, (C) Overlay map, (D) Carbon map, (E) oxygen map, (F) fluorine map, (G) sulfur map and (H) EDX spectrum and the inset shows the composition analysis.

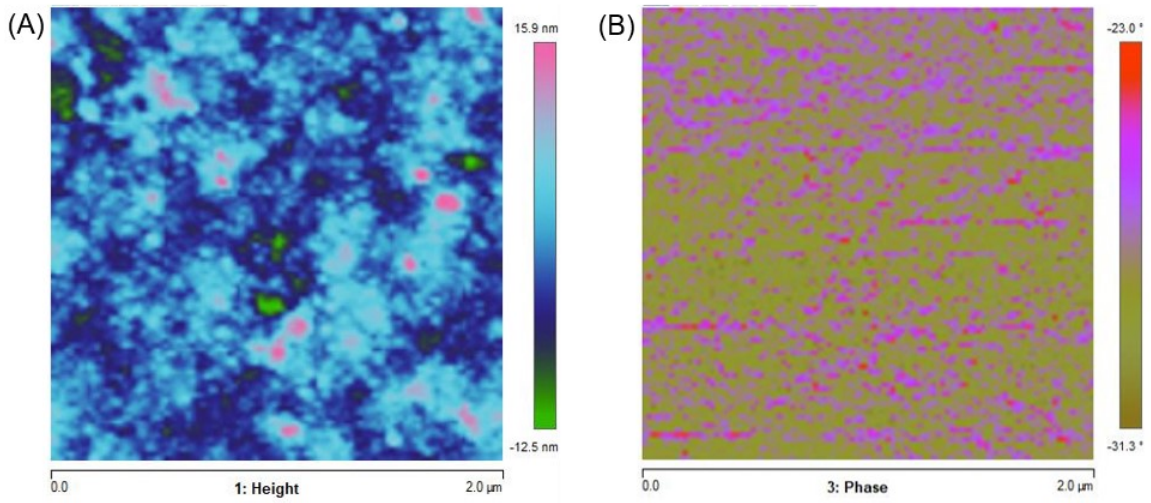

Figure S2. Atomic force microscopic images of Nafion membrane (A) 2D topographic image, and (B) Phase image.

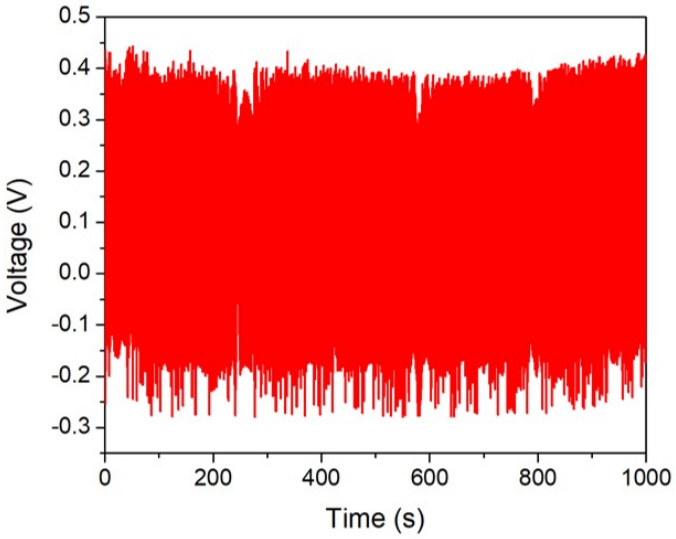

Figure S3. Electro-mechanical stability of the Nafion polyelectrolyte film over 1000 seconds.

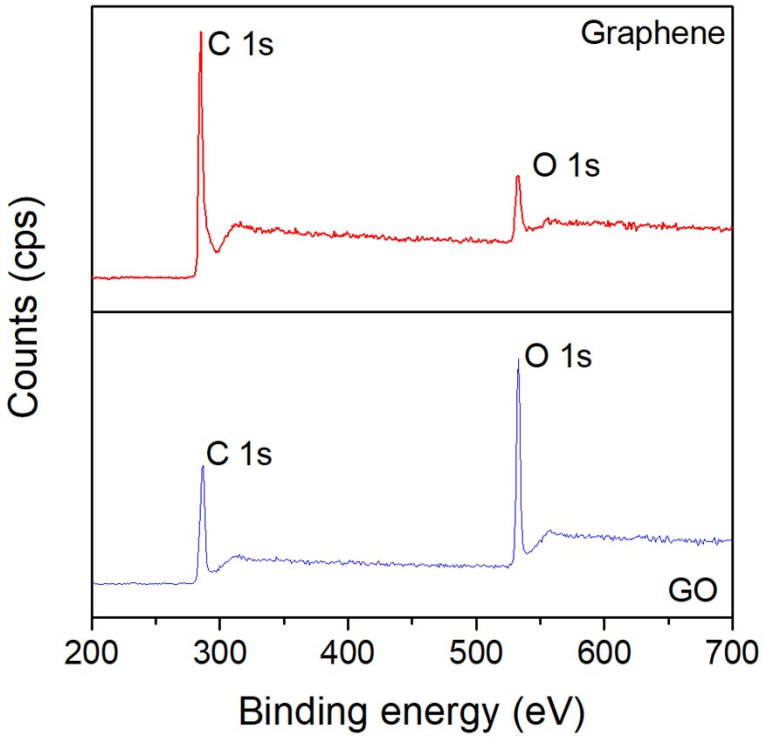

Figure S4. X-ray photoelectron spectroscopy survey scans of GO and graphene sheets.

The X-ray photoelectron spectra of GO and graphene sheets (Figure S4) shows the presence of C 1s and O 1s at 284.5 and 531.5 eV, respectively. Additionally, the intensity of O 1s is decreased in graphene sheets compared to GO sheets which confirms the reduction of GO into graphene sheets [1].

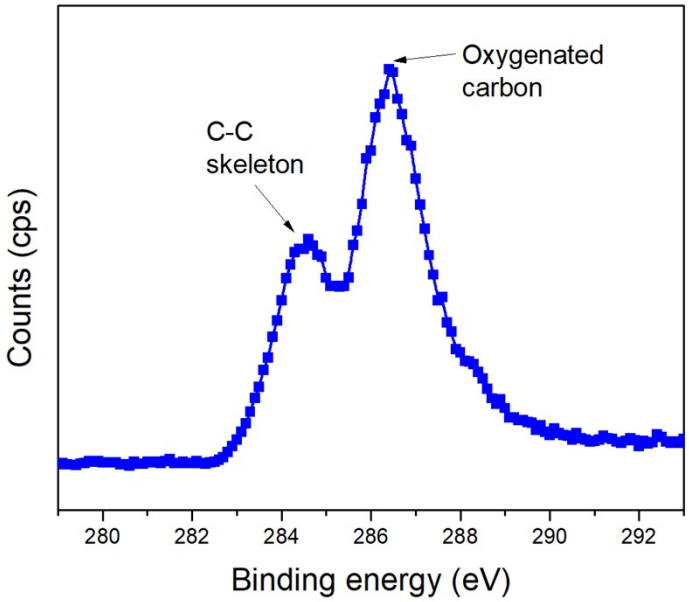

Figure S5. X-ray photoelectron C 1s spectrum of GO sheets.

The core-level C 1s spectrum of GO sheets (Figure S5) show the presence of C-C skeleton (284.5 eV), and carbon bonded with oxygenated functional groups ((286.1 To 289.8 eV), which indicated the graphite is oxidized into graphene oxide via the modified Hummers method [4].

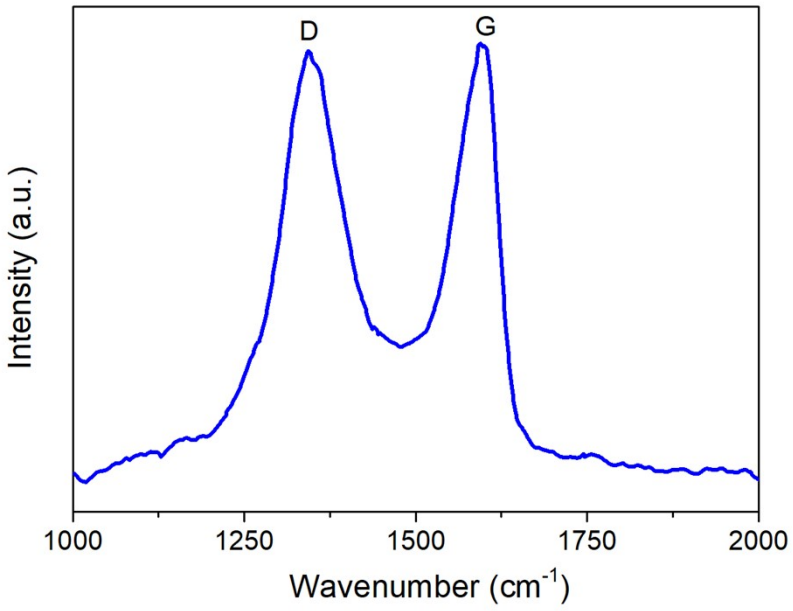

Figure S6. Raman spectrum of GO sheets.

The Raman spectrum of GO sheets (Figure S6.) show the presence of D and G band at 1350 cm-1 and 1598 cm^{-1}, respectively. In comparison to the G band of graphite (usually appears at 1575 cm^{-1}), the G band of GO shifts towards the higher wavenumber which is due to the oxidation of graphite [2].

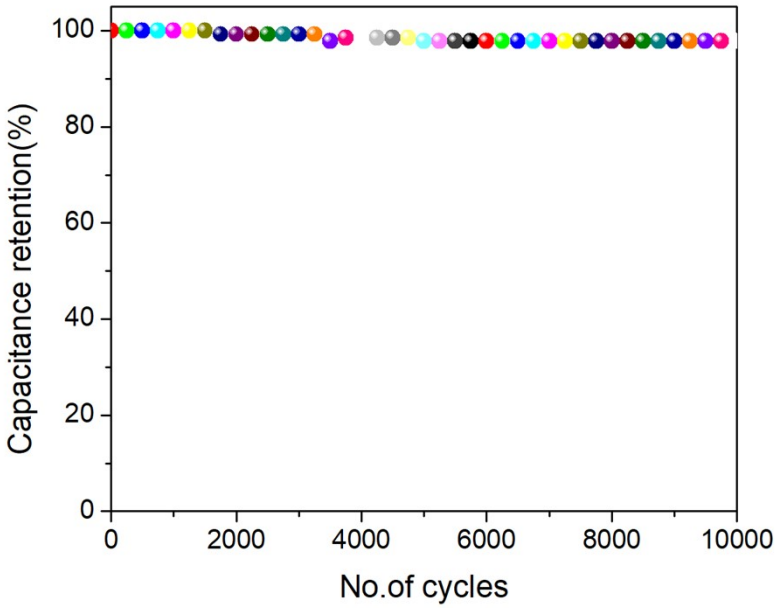

Figure S7. Stability of graphene PI-SCSPC.

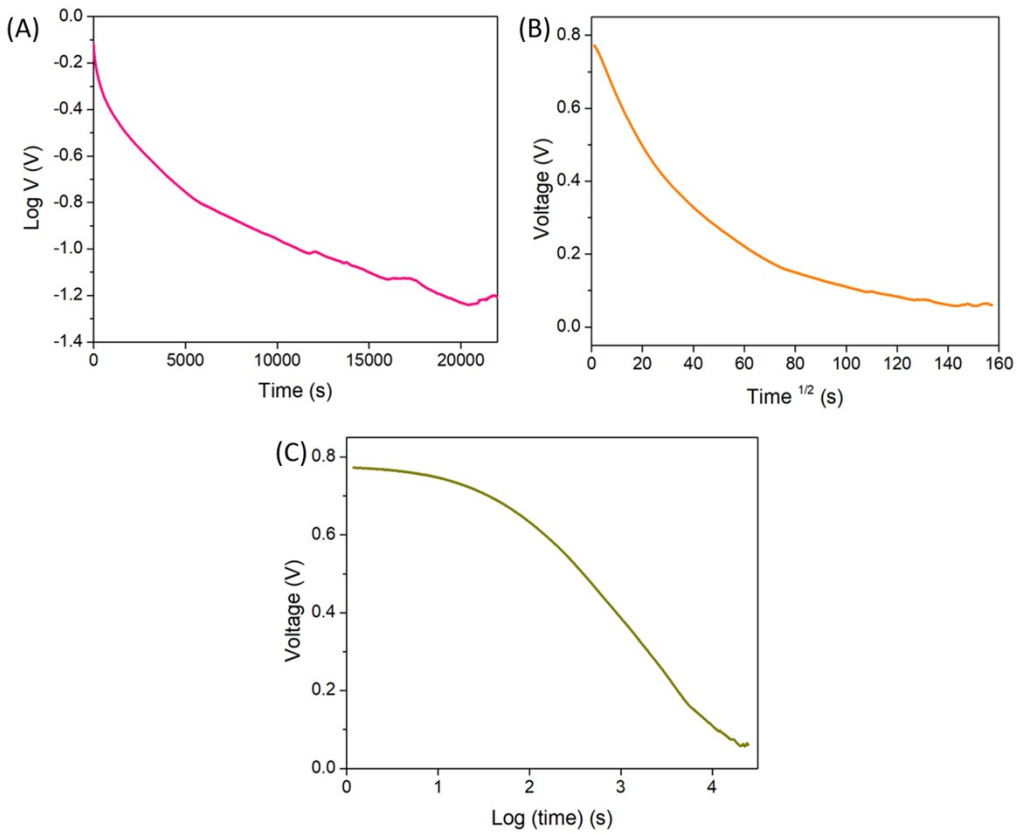

Figure S8. Fitting for self-discharge analysis.

In general, self-discharge of a supercapacitor can occurred due to (i) ohmic leakage, (ii) diffusion mediated pathways, (iii) overcharging issues, respectively[3,5]. To explore the mechanism of self-discharge in graphene PI-SCSPCs (given in Figure 3(H)), the experimental data is fitted as shown in Figure S5. The plot of log V versus t (Figure S5(A)) shows the non-linear profiles which suggested that ohmic leakage is not only the reason for the observed self-discharge. The plot of V versus $t^{1/2}$ (Figure S5(B)) showed that the role of diffusion mediated process in the involvement of self-discharge process. The observation of non-linear curves in the plot of voltage versus log (time) (Figure S5(C)) confirms that there is no involvement of any overcharging issues in the observed self-discharge [6].

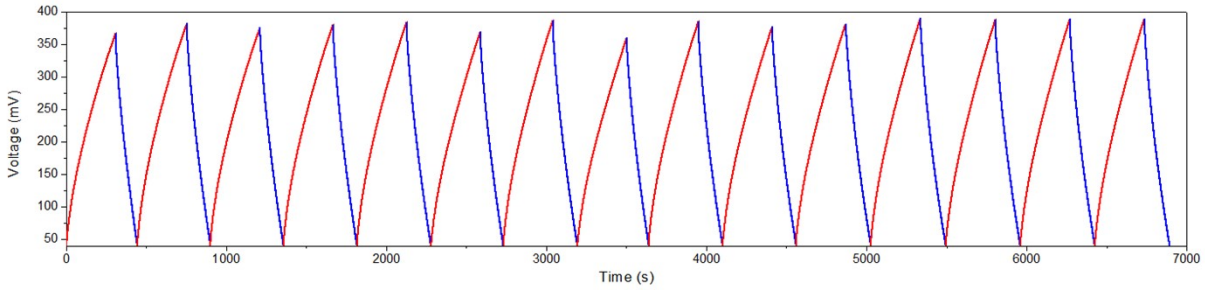

Figure S9. Stability of the self-charging properties of the graphene PI-SCSPC subjected to a continuous compressive force of 15 N.

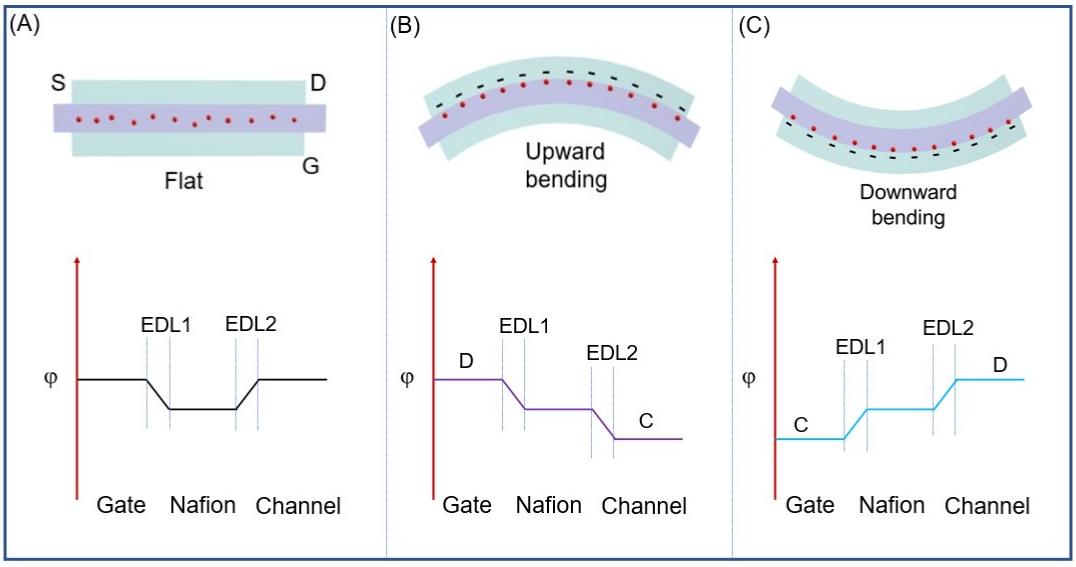

Figure S10. Potential distribution diagram of graphene PI-SCSPC at (A) flat conditions, (B) upward bending, and (C) downward bending states, respectively.

Table S1: Energy and power density performance of Graphene PI-SCSPC compared to reported SCs.

S. No.	Electrode	Electrolyte	Energy density ($\mu Wh\ cm^{-2}$)	Power density ($mW\ cm^{-2}$)	Ref
1.	SIC nanowires	PVA/KCl	5.24	11.2	[7]
2.	RGO+CNT@CMC	PVA/H_3PO_4	3.84	0.02	[8]
3.	MWCNT/OMC	PVA/H_3PO_4	1.77	0.004	[9]
4.	I-Ti_3CTx	PVA/H_2SO_4	0.76	0.33	[10]
5.	SIC NWs	Yttria-stabilized Zirconia	0.1	0.01	[11]
6.	Reduced Graphene oxide	H_2SO_4	4.1	5	[12]
7.	CNT/MnO_2/Polymer	PVA/LiCl	2.6	0.2	[13]
8.	Carbyne enriched carbon	PVA/H_2SO_4	0.1	2.2	[14]
9.	Graphene	H_2SO_4	1.24	24.5	[15]
10.	TiC_2 MXene	H_2SO_4	0.21	3.34	[16]
11.	**Graphene**	**Nafion solid polyelectrolyte**	**21.78**	**0.888**	**This work**

Table S2: Self-charging performance of Graphene PI-SCSPC using Nafion polyelectrolyte compared to reported SCSPCs utilizing piezopolymer and piezo-ceramic separators.

S. No	Material	Electrolyte	Separator	Charging voltage	Reference
SCSPCs using piezo-polymer separator					
1	MnO_2	PVA/H_3PO_4	PVDF/ZnO	110 mV	[17]
2	Carbon	PVA/H_2SO_4	Polarized PVDF	100 mV	[18]
3	Carbon nanotubes	$PMMA/LiClO_4$	PVDF-TrFE	70 mV	[19]
4	NiCo(OH) // graphene ASC	PVA/KOH	Fish swim bladder	153 mV	[20]
6	Graphene	$TEABF_4$	Porous PVDF	112 mV	[21]
7	Siloxene	PVDF-co-HFP/$TEABF_4$	Electrospun PVDF/Siloxene	207 mV	[22]
8	MnO_2-rGO	$PVA-H_3PO_4$	PVDF-ZnO-RGO	~190 mV	[23]
SCSPCs using piezo-ceramic separator					
9	Graphene/SEBS	PVA/H_3PO_4/KNN		110 mV	[24]
10	$NiCo_2O_4$@ACC	PVA/KOH/$BaTiO_3$		225 mV	[25]
11	Fe_2O_3@ACC	PVA/KCl/$BaTiO_3$		120 mV	[26]
12	Graphene/CC	PTA/PVDF		110 mV	[27]

13	**Graphene PI-SCSPC**	**Nafion solid polyelectrolyte**	**341 mV**	**This work**

References:

1 K. Krishnamoorthy, M. Veerapandian, K. Yun and S.-J. Kim, *Carbon N. Y.*, 2013, **53**, 38–49.

2 S. Manoharan, K. Krishnamoorthy, A. Sathyaseelan and S.-J. Kim, *Mater. Chem. Front.*, 2021, **5**, 6200–6211.

3 K. Krishnamoorthy, P. Pazhamalai, V. K. Mariappan, S. Manoharan, D. Kesavan and S. Kim, *Adv. Funct. Mater.*, 2021, **31**, 2008422.

4 K. Krishnamoorthy, G.-S. Kim and S. J. Kim, *Ultrason. Sonochem.*, 2013, **20**, 644–649.

5 M. A. Bissett, I. A. Kinloch and R. A. W. Dryfe, *ACS Appl. Mater. Interfaces*, 2015, **7**, 17388–98.

6 S. Manoharan, K. Krishnamoorthy, V. K. Mariappan, D. Kesavan and S.-J. Kim, *Chem. Eng. J.*, 2021, **421**, 129548.

7 W. Li, Q. Liu, Z. Fang, L. Wang, S. Chen, F. Gao, Y. Ji, W. Yang and X. Fang, *Adv. Energy Mater.*, 2019, **9**, 1–8.

8 L. Kou, T. Huang, B. Zheng, Y. Han, X. Zhao, K. Gopalsamy, H. Sun and C. Gao, *Nat. Commun.*, 2014, **5**, 3754.

9 J. Ren, W. Bai, G. Guan, Y. Zhang and H. Peng, *Adv. Mater.*, 2013, **25**, 5965–70.

10 C. J. Zhang, M. P. Kremer, A. Seral-Ascaso, S. H. Park, N. McEvoy, B. Anasori, Y. Gogotsi and V. Nicolosi, *Adv. Funct. Mater.*, 2018, **28**, 1–10.

11 C. H. Chang, B. Hsia, J. P. Alper, S. Wang, L. E. Luna, C. Carraro, S. Y. Lu and R.

Maboudian, *ACS Appl. Mater. Interfaces*, 2015, **7**, 26658–26665.

12 U. N. Maiti, J. Lim, K. E. Lee, W. J. Lee and S. O. Kim, *Adv. Mater.*, 2014, **26**, 615–619.

13 C. Choi, S. H. Kim, H. J. Sim, J. A. Lee, A. Y. Choi, Y. T. Kim, X. Lepró, G. M. Spinks, R. H. Baughman and S. J. Kim, *Sci. Rep.*, 2015, **5**, 1–6.

14 V. K. Mariappan, K. Krishnamoorthy, P. Pazhamalai and S.-J. Kim, *Mater. Adv.*, 2020, **1**, 1644–1652.

15 Z. Xiong, C. Liao, W. Han and X. Wang, *Adv. Mater.*, 2015, **27**, 4469–4475.

16 N. Kurra, B. Ahmed, Y. Gogotsi and H. N. Alshareef, *Adv. Energy Mater.*, 2016, **6**, 1601372.

17 A. Ramadoss, B. Saravanakumar, S. W. Lee, Y.-S. Kim, S. J. Kim and Z. L. Wang, *ACS Nano*, 2015, **9**, 4337–4345.

18 R. Song, H. Jin, X. Li, L. Fei, Y. Zhao, H. Huang, H. Lai-Wa Chan, Y. Wang and Y. Chai, *J. Mater. Chem. A*, 2015, **3**, 14963–14970.

19 K. Parida, V. Bhavanasi, V. Kumar, J. Wang and P. S. Lee, *J. Power Sources*, 2017, **342**, 70–78.

20 A. Maitra, S. K. Karan, S. Paria, A. K. Das, R. Bera, L. Halder, S. K. Si, A. Bera and B. B. Khatua, *Nano Energy*, 2017, **40**, 633–645.

21 S. Sahoo, K. Krishnamoorthy, P. Pazhamalai, V. K. Mariappan, S. Manoharan and S.-J. Kim, *J. Mater. Chem. A*, 2019, **7**, 21693–21703.

22 K. Krishnamoorthy, P. Pazhamalai, V. K. Mariappan, S. S. Nardekar, S. Sahoo and S.-J. Kim, *Nat. Commun.*, 2020, **11**, 2351.

23 A. Rasheed, W. He, Y. Qian, H. Park and D. J. Kang, *ACS Appl. Mater. Interfaces*, 2020, **12**, 20891–20900.

24 D. Zhou, N. Wang, T. Yang, L. Wang, X. Cao and Z. L. Wang, *Mater. Horizons*, 2020, **7**, 2158–2167.

25 D. Zhou, F. Wang, X. Zhao, J. Yang, H. Lu, L.-Y. Lin and L.-Z. Fan, *ACS Appl. Mater. Interfaces*, 2020, **12**, 44883–44891.

26 D. Zhou, F. Wang, J. Yang and L. Fan, *Chem. Eng. J.*, 2021, **406**, 126825.

27 S. Manoharan, P. Pazhamalai, V. K. Mariappan, K. Murugesan, S. Subramanian, K. Krishnamoorthy and S.-J. Kim, *Nano Energy*, 2021, **83**, 105753.